CHAPTER 9

Modeling and Simulations of Multicomponent Hydrogels for Biomedical Applications

IONEL POPA

Department of Physics, University of Wisconsin-Milwaukee,
3135 N. Maryland Ave, Milwaukee, WI 53211, USA
Email: popa@uwm.edu

9.1 Overview

Modeling of multicomponent hydrogels has the potential to predict novel properties and biomedical applications while describing their complex response from the nanoscopic to the macroscopic scale. Typically multicomponent hydrogels use networks with contrasting properties, such as brittle/ductile,[1] and combine various functions, such as stiffness, with biofunctionality. Another advantage of multicomponent hydrogels stems from the fact that they can show large enhancements related to their elastic range (range of stresses from which materials recover their initial structure) and toughness (ability to absorb energy and withstand shock before fracture), as one network can act as support and another as sacrificial.[2]

Modeling and simulation studies of multicomponent hydrogels typically follow their experimental implementations and aim to further optimize their function and better understand their response. There are four main classes of multicomponent hydrogels which will be the subject of this chapter: (i) polymer–polymer, (ii) polymer–protein, (iii) polymer–inclusion and (iv) void

Biomaterials Science Series No. 15
Multicomponent Hydrogels: Smart Materials for Biomedical Applications
Edited by Jagan Mohan Dodda, Kalim Deshmukh and Deon Bezuidenhout
© The Royal Society of Chemistry 2023
Published by the Royal Society of Chemistry, www.rsc.org

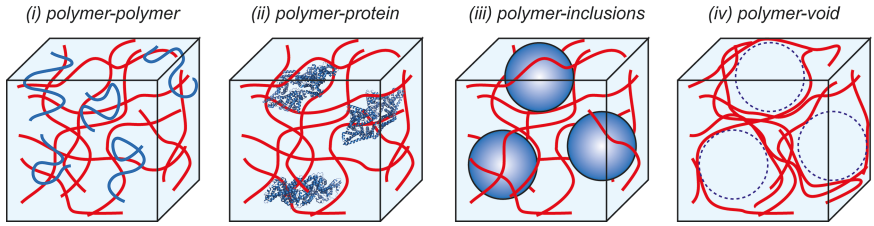

Figure 9.1 Types of multicomponent hydrogels discussed in this chapter. (i) Polymer–polymer hydrogels use synergistic properties from their individual components to improve various properties; (ii) polymer–protein biomaterials combine natural proteins with man-made polymers; (iii) polymer–inclusions use non-dissolvable particles inside a polymer matrix; (iv) polymer–void double networks have one of the networks removed after synthesis.

double-network (DN) hydrogels (Figure 9.1). While experimentally there have been reports of multicomponent hydrogels with more than two percolating networks,[3] the vast majority are double network (DN) hydrogels, which will be the main focus here.

(i) Polymer–polymer hydrogels are the most common implementation of multicomponent materials. They typically show synergetic properties from their individual components, and in some cases the overall response exceeds the sum of their components. Polymer–polymer hydrogels can provide a hydrated environment for cells and have been used for cell growth as well as for filtration and biosensing.[4] Furthermore, polymer-based composite hydrogels use a secondary filler network to enhance their mechanical strength or maintain high elasticity while also displaying high porosity.[5] The secondary network can not only act as a reinforcer, but also provide self-healing capabilities to the hydrogel.[6] Among the numerous implementations, hydrogels synthesized with poly(2-acrylamido-2-methylpropanesulfonic acid) (PAMPS)/polyacrylamide (PAM) stand out due to their exceptional mechanical properties. PAMPS is a negatively charged polyelectrolyte, while PAM is a neutral polymer.[7,8] At an optimal ratio, the PAMPS/PPM mixture shows a tearing energy greater than the summation of its individual components and compression fracture comparable to cartilage.[7,8]

(ii) Polymer–protein and protein–polymer multicomponent hydrogels can harvest from the biodiversity of proteins and the large availability of polymers.[9] They easily enable controlled drug release[10] and can provide an ideal matrix for cell growth.[11,12] Experimentally, there are many implementations of such materials, with unique properties. For example, a peptide amphiphile and a 1,3:2,4-dibenzylidene-*d*-sorbitol (DBS) gelator were shown both experimentally and through modeling

to self-assemble into nano-fibers.[13] Also naturally-occurring polysaccharides like chitosan, alginate or cellulose have been extensively used to retain proteins.[14,15] The vast majority of hydrogels that have proteins and polymers as components have the polymer molecules forming the primary network and adsorbed proteins as their secondary network. The reasoning behind this approach comes from the fact that polymers are both cheaper and easier to produce than proteins.

Back in 2010, a photochemical crosslinking approach was implemented by Li and collaborators that allowed most proteins with exposed tyrosine amino acids to form covalent carbon–carbon bonds, while maintaining their folded structures.[16] This approach enabled proteins to become part of the primary network of multicomponent hydrogels. The protein molecules can be either in monomeric form or engineered with several repeats (typically up to eight repeating domains, limited by the used bacterial expression system). Modeling and simulations of the cross-linking of protein hydrogels captured the intrinsic random arrangement of molecules, as well as their orientation and unfolding under a force vector.[17,18] Recently, experimental demonstrations of multicomponent hydrogels with proteins as their primary network were reported in conjugation with other proteins,[18,19] polyelectrolytes[20] or small ions.[21,22] Unlike purely polymeric hydrogels, protein-based materials have an added level of complexity coming from the unfolding and refolding of protein domains, which can be driven by force, temperature, or chemical denaturants. This property can be used to induce shape memory[19,20] or influence the energy dissipation of the material.[16,23]

(iii) Polymer–inclusion or polymer–particle hydrogels use insoluble structures that have often spherical or cylindrical geometry to produce composites with enhanced properties. They are relatively easy to produce and require a good adhesion between the inclusion and the polymeric matrix. Examples of such approaches use nanocrystals,[24,25] carbon nanotubes,[26,27] metal nanoparticles,[28,29] magnetic beads,[30,31] and silica particles.[32,33] Nanoclays have been used in composite hydrogels as reinforcers and as initiators for cross-linking.[34,35]

(iv) Void hydrogels use a dissolvable secondary network, which is removed after cross-linking. These multicomponent hydrogels can show reinforced mechanical strength and toughness, and enhanced permeability, and can accommodate cells.[36,37] Furthermore, they provide an ideal medium for the understanding of the mesoscale fracture mechanism in DN systems.[1] In one such approach, silica beads of varying sizes and densities were added into solution before cross-linking the primary network.[36] The beads were then dissolved using hydrofluoric acid, leaving behind hollow void structures. Both the fracture energy and elasticity of these void-DN gels depend on the

size and density of the voids, and were assigned to partial concentration of stress near the void structure.[36] Another approach used a spiropyran-based light-responsive polymer (EPS) in combination with alginate–polyacrylamide (ALG–PAAm) interpenetrating hydrogels.[38] Following crosslinking of the three components, EPS was converted from gel to sol under UV light, leaving vacancies in the material network. In another implementation, alginate was used as the porogen for bovine serum albumin (BSA)-based hydrogels.[39] In this case, BSA cross-linking was initiated *via* a light activated reaction while immersed in alginate solution. Following a short exposure and while still under light, the biomaterial was immersed in Ca^{2+}, which led to the competitive formation of alginate aggregates. Removal of Ca^{2+} left behind pores of ~5 μm diameter throughout the biomaterial.[39]

9.2 Overview of Modeling Approaches for Multicomponent Hydrogels

Modeling techniques aim to present a detailed picture of multicomponent materials that matches their experimentally measured characteristics. Among these characteristics, the mechanical response of hydrogels is most informative, and it is typically obtained under tensile or compressive stress. Arguably, tensile or tearing tests are more representative of the true toughness of a material.[1] Experimentally, it is easier to study the mechanical response of materials by applying a constant or linearly increasing strain, which simply requires the movement of one of the tethered ends and measurement of the developed stress by the material. This approach, where the stress of a material is measured over time at a controlled displacement, is known as length-clamp or stress-relaxation test. However, most multicomponent hydrogels show a viscoelastic response related to a molecular change, such as sliding of network components, breaking of local interactions or even phase transitions.[40] This time-dependent response makes it challenging to separate the change in internal force, due to molecular movements, from hydrogel extension with time, and does not constitute an ideal scenario for developing and testing theoretical models. Hence, from a modeling perspective, it is very important to control the applied stress rather than the applied strain. Such a feat can be achieved if the measuring device has an active feedback mechanism, which measures the stress exerted on the material and continuously adjusts the strain to match a specific set-point.[23,41] This approach, where the strain experienced by the material is measured over time at a constant force, is known as constant force-clamp or creep-relaxation test.

Modeling and simulations of multicomponent hydrogels require a multiscale approach (Figure 9.2). When implementing a model of a material, improvements in resolution and accuracy come at the expense of computational time. Hence, when scale is of the essence, more approximations are

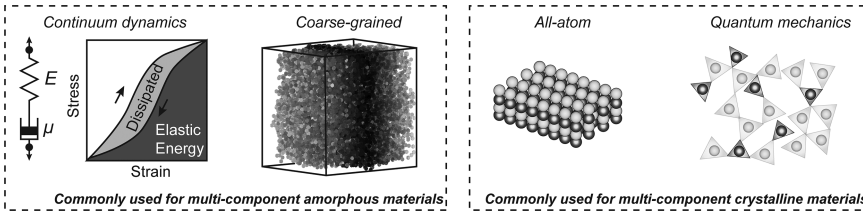

Figure 9.2 Modeling of biomaterials on different scales. Continuum models and coarse-grained approaches can describe the behavior of multicomponent amorphous materials, while all-atom and quantum-mechanics based models are better suited for multicomponent crystalline materials.

needed to maintain reasonable computational times. Based on their level of detail, the modeling techniques can be classified from continuum dynamics all the way to quantum mechanics. Here we will only reference a few of these models, and for a more in-depth description we refer the reader to other excellent reviews.[42,43]

Continuum dynamics models use process time-dependent and independent variables to describe a macroscopic behavior as a function of a constant or varying perturbation. Such processes take place on a time scale of seconds to minutes and on physical dimensions of microns to millimeters (or more). Several continuum models have been developed and successfully applied to characterize the response of multicomponent hydrogels to an applied strain.[43,44] They typically rely on combinations of purely elastic elements, such as springs, and visco-elastic components that can incorporate the time-dependent response, such as dashpots. More complex models allow investigation of the effects of molecular orientation and end-to-end distance distribution on the mechanical properties of a material.[45,46] Finally, macroscopic models have also been developed to explain the irreversible softening during cyclic loading–unloading stress–strain cycles by considering structural alterations, where the primary and/or secondary network can break and reform.[47–49]

Coarse-grained models divide molecules and molecular structures into abstracted components, without retaining their atomic details. These methods map the arrangement and dynamics of the molecules, agglomerates and aggregates forming a multicomponent material.[50–52] Typically molecules are represented as hard or soft spheres. The simulations use Newtonian dynamics and potential energy to describe the motion of the grains over large time steps, of nano- to picoseconds. These models bridge the molecular scale to the macroscale and can capture large-scale behaviors, by using force-fields or Langevin dynamics.[53–55] Force fields can generally provide a more in-depth view, as they assign specific parameters to grains, such as polarity, charge, or hydrogen-bonding ability, but they do so at the expense of computational time. The main challenge when transitioning from a material to its coarse-grained representation arises from the large

number of molecules (10^{10}–10^{20} molecules per gram) and the intrinsically slow time scales (typically seconds to minutes) required for synthesis and characterization of biomaterials, which are at odds with molecular modeling and simulations that typically investigate few molecules (10^2–10^5 molecules) over short time scales (nanoseconds to microseconds). While these studies are more challenging to perform and make predictions over smaller time scales, they are important because of the mechanistic view provided and from the potential predictions on how the properties of materials can be altered as a function of the nature and ratio of their components and response to a specific stimulus.

Further details at the atomic and electronic levels can be obtained *via* molecular dynamics (MD) simulations of atoms. MD simulations of atoms use fields to represent the interaction energy between atoms and can account for both intra- and intermolecular interfaces.[56,57] These methods provide molecular details related to the rotation, vibration and translation of bonds forming a network. MD simulations operate on the nano-to-microsecond time scale, over nanometer distances, and can have even 10^{10} number of atoms.[56,58]

All-atom and quantum mechanics simulations are essential for studying chemical reactions and energetically excited states, but they are typically limited to less than 10^3 atoms on timescales of picoseconds.[59] Multicomponent hydrogels are many orders of magnitude larger, are anisotropic, and respond on timescales of minutes to hours. Hence, these approaches are more appropriate for multicomponent materials with repeating unit structures, such as crystalline materials, and are less common when characterizing randomly structured materials (Figure 9.2).

In this chapter we will focus our discussion on the use of macroscopic continuum and nanoscopic coarse-grained models to describe multicomponent hydrogels with different network compositions.

9.3 Macroscopic Continuum Dynamics Models

Macroscopic continuum models use the physics of springs and dashpots to represent the elastic and visco-elastic responses of materials. The placement of these elements in series, parallel, or various series–parallel combinations results in specific behaviors and can be related to various parts of multicomponent hydrogels.[60] Several such models are depicted in Figure 9.3, together with their expected strain response over time, when experiencing a constant force (or stress).

The Maxwell model considers a spring in series with a dashpot (Figure 9.3A, top-left), and, at constant stress, σ, the strain, ε, will first show a fast change due to the spring element, which quickly reaches equilibrium, followed by the slower extension due to viscoelasticity:

$$\varepsilon(t) = \left(\frac{1}{E} + \frac{t}{\mu}\right) \cdot \sigma \tag{9.1}$$

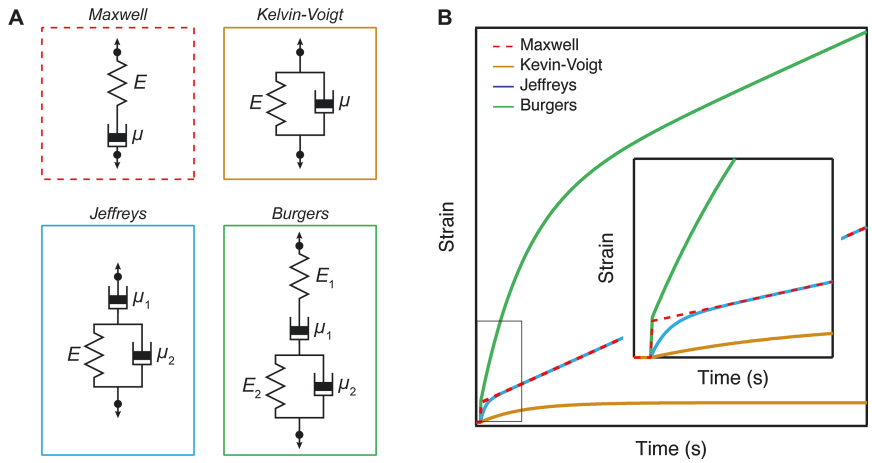

Figure 9.3 Viscoelasticity models representative of biomaterials. (A) (top) Two-element models of spring and dashpot in series (Maxwell) and parallel (Kelvin–Voigt); (bottom) three- (Jeffreys) and four- (Burgers) element models. (B) Predicted creep (strain *vs.* time) by the models in (A) for a constant stress. Inset: Zoom-in of the initial creep part.

where E is Young's modulus, μ is the material coefficient of viscosity, and t is time.

The Kevin–Voigt model predicts the mechanical response of a spring in parallel to a dashpot (Figure 9.3A, top-right). In this case, the dynamics of the overall extension are regulated by the slow response of the dashpot and given by

$$\varepsilon(t) = \left[1 - \exp\left(-\frac{E}{\mu}t\right)\right] \cdot \frac{\sigma}{E} \tag{9.2}$$

Three-component representations can have either two springs and one dashpot (Zener model), or two dashpots and one spring (Jeffreys model). When a dashpot is placed in series with a spring/dashpot in parallel, the Jeffreys representation (Figure 9.3A, bottom-left) predicts a change in strain with time at a constant stress as

$$\varepsilon(t) = \left[\frac{1}{E} + \frac{t}{\mu_1} - \frac{1}{E} \cdot \exp\left(-\frac{E}{\mu_2}t\right)\right] \cdot \sigma \tag{9.3}$$

where μ_1 is the coefficient of viscosity for the dashpot in series and μ_2 the coefficient of viscosity for the dashpot in parallel with a spring.

Finally, four-component models have springs and dashpots in various serial–parallel configurations. For example, the Burgers models extend the Maxwell and Kevin–Voight representations. For multicomponent hydrogels,

the Kelvin representation of this model is shown above (Figure 9.3A, bottom-right). In this representation, a serial spring–dashpot is placed in series with a parallel spring/dashpot. Given distinctive Young's moduli, E_1 and E_2, and coefficients of viscosity, μ_1 and μ_2, the expected change in strain at a constant stress is

$$\varepsilon(t) = \left\{1 + \frac{E_1}{\mu_1} \cdot t + \frac{E_1}{E_2}\left[1 - \exp\left(-\frac{E_2}{\mu_2}t\right)\right]\right\} \cdot \frac{\sigma}{E_1} \tag{9.4}$$

When plotting the creep, the Kelvin–Voigt model (spring–dashpot in parallel) shows an exponential increase in strain with time at constant stress, dominated by the viscous element (Figure 9.3B). When the spring and dashpot are in series (Maxwell), the response is dominated initially by the spring. As more elements are added, the response becomes more complex. As typically double-network materials have a response originating from their single-network components, models with three (Jeffreys) or four elements (Burgers or Kelvin–Voigt for four elements) are better suited to describe their response from a macroscopic perspective.

An interesting aspect of current macroscopic models originates from the fact that the spring element is typically treated as having a linear response of extension as a function of force over the entire force range (Hookean spring). It is well-known from polymer physics that the extension of a macromolecule under a force is only linear in the low force regime (typically less than 10 pN per molecule). At high forces, the extension becomes non-linear, due to the high entropic cost required to extend a polymeric chain, as well as the rigidity of the covalent bonds forming the molecular backbone. Hence, the behavior of a macromolecule under force can be described by polymer elasticity models, such as the freely jointed chain (FJC):[61]

$$\frac{x}{L_c} = \coth\left(\frac{Fl}{kT}\right) - \frac{kT}{Fl} \tag{9.5}$$

where x is the extension, L_c the contour length, F the force, l the bond (Khun) length and kT the thermal energy (Figure 9.4A, black trace). For low forces, the first term can be Taylor-expanded as $\coth(a) = \frac{1}{a} + \frac{a}{3} + \ldots$, and eqn (9.5) becomes

$$\frac{x}{L_c} \approx \frac{l}{3kT} f \tag{9.6}$$

which resembles the behavior of a Hookean spring (Figure 9.4A, red *vs.* blue traces).

The fact that a polymer molecule cannot extend beyond its contour length without breaking its backbone may become important at high forces-per-molecules, as the extension is plateauing asymptotically toward the contour length. These high forces are typically not attainable with a single network material, but are measured experimentally for DN hydrogels. Hence, if one

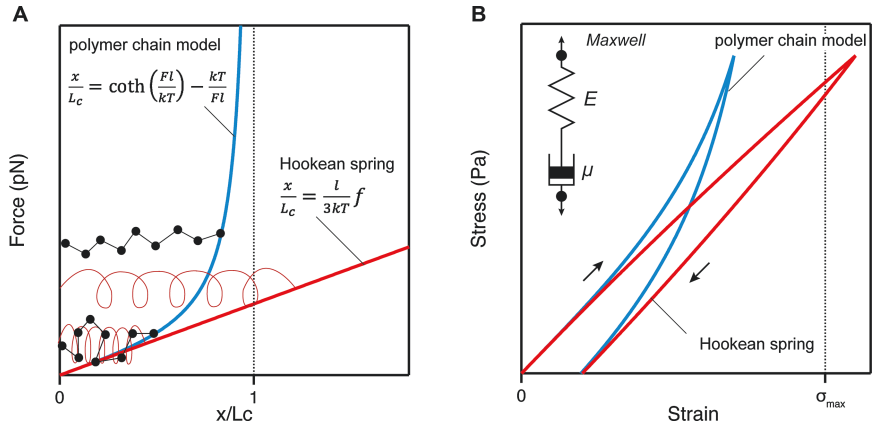

Figure 9.4 Moving beyond Hookean springs to represent continuum models. (A) Change in extension of a macromolecule x normalized by contour length L_c as a function of force, calculated using a freely-jointed chain (FJC) model for the elasticity of a polymeric chain (blue curve) and the low-force approximation (red line, which resembles a Hookean spring). Schematics show extension of a spring and a molecule. (B) Stress-*vs.*-strain for the Maxwell representation, assuming a Hookean spring (red trace) and a polymer chain (blue trace), with maximum strain of σ_{max}. Arrows indicate the change with time.

considers the non-linear response of macromolecules at medium to high forces, the strain will plateau with stress (Figure 9.4B). As covalent bonds are inelastic, after alignment to a force vector, the molecules inside the material can no longer extend without breaking. Such an asymptotic change of stress with strain, also known as densification or orientational hardening, has been reported experimentally for DN gels made from cellulose/gelatin,[62] poly(2-acrylamido-2-methylpropanesulfonic acid) (PAMPS)/polyacrylamide (PAAm),[63] or from poly(ethylene glycol) (PEG)/poly(acrylic acid) (PAA).[64] Interestingly, they have not been interpreted as arising from polymer-extensibility limitations.

(i) Polymer–polymer multicomponent hydrogels have been often characterized with continuum models. One effort, where macroscopic continuum models were lucratively applied to describe multicomponent hydrogels, involved the synthesis of artificial extracellular matrix (ECM) proxies.[12] The ECM is a multicomponent environment made from insoluble proteins and sugar molecules secreted by cells, and it provides both structural and chemical support. More importantly, the stiffness of the ECM is critically important for the survival and proliferation of specialized cells, which signal cells to divide, function normally, or undergo apoptosis.[65] Using covalent coupling between PEG spacers and alginate molecules and changes in the molecular size of alginate, Mooney and collaborators managed, in the

presence of Ca^{2+} ions, to produce hydrogels with adjustable stress-relaxation rates.[12] These materials showed stress-relaxation behavior that was well described by a two-element Maxwell–Weichert linear viscoelastic model (two serial spring–dashpot elements in parallel) and could not be fitted with a simple Maxwell model (single serial spring–dashpot). The multi-characteristic relaxation timescales were attributed to different molecular interactions and correlated with the size distribution of the building blocks.

(ii) Protein–polymer and protein–protein based materials have been often modeled with continuum approaches. Most biological tissues are naturally-occurring multicomponent networks and their behavior was described using all of the models mentioned above.[66–69] Continuum models were also used to report material nonlinearity measured for fibrous structures, such as those based on fibrin and collagen.[70–72] In a study focusing on collagen, which is the most abundant protein in the human body, the authors determined the importance of different parameters of the fibrous network on their mechanical response.[70]

(iii) Biomaterials made with polymer–inclusions, such as nanoparticles, can show high stretchability and toughness. A constitutive model having nanoparticle crosslinkers was proposed considering the varying lengths of the polymer molecules attached between particles.[73] While this model only considers the elasticity of the polymer–particle crosslinks and ignores interactions between entangled polymer chains, it manages to capture the effects of chain detachment from particles and the influence of the particle size on the cyclic mechanical response of nanocomposite hydrogels. In a different approach, a model titled ''the polymer reference interaction site model'' uses density correlation functions to predict the structure of polymer–nanoparticle mixtures.[74]

(iv) Void-double network materials have also been studied using macroscopic modeling. For example, the poro-viscoelastic behavior of agarose gels was investigated using a generalized Maxwell model.[75] Agarose gels can be formulated to have precise and homogenous pore sizes, which in turn allow for diffusion of large molecules, such as DNA or proteins.[76] Not only do different formulations produce different pore sizes, but the viscoelasticity of agarose gels changes significantly with pore size. This feature was used experimentally to match the elasticity of biological tissues and induce cellular differentiation based on substrate mechanics.[77,78] The authors described the behavior of agar gels when having only solvent-percolated pores and when a drug was loaded throughout the material.[75] In another study, a macroscopic modeling approach was developed to describe the swelling of a multi-phasic material undergoing mass transfer.[79] The multi-phasic porous hydrogel was modified with a material made from superabsorbent polymers and a three-phase model was developed to account for absorption and desorption processes and swelling-dependent permeability.

9.4 Nanoscopic Models of Multicomponent Hydrogels

Unlike continuum macroscopic network models, discrete nanoscopic models can capture specific features, such as network disorder, heterogeneities and anisotropy. The large majority of nanoscopic models for multicomponent hydrogels use coarse-grained approaches, which can represent the system on longer length and time scales than atomistic and quantum mechanics-based approaches. These methods can have various degrees of coarse-graining depending on the number of atoms represented by a grain. Most coarse-grained methods consider the Brownian motion of particles, which can be described using the Langevin equation:

$$m_i \frac{\mathrm{d}^2 r_i}{\mathrm{d}t^2} = -\eta \frac{\mathrm{d}r_i}{\mathrm{d}t} + f_i + \Gamma(t) \tag{9.7}$$

where m_i and r_i are the mass and position of a particle i, t is time, and f_i is the sum of the forces exerted on the particle. The friction coefficient η can be related to the diffusion coefficient D as $\eta = D/kT$. The random force inducing the Brownian motion $\Gamma(t)$ is characterized by a Gaussian distribution with $\langle \Gamma(t) \rangle = 0$, which satisfies the fluctuation–dissipation relation $\langle \Gamma(t)\Gamma(t') \rangle = 2\eta kT\delta(t - t')$, where $\delta(t - t')$ is the Dirac delta function. Typically the inertia term on the left-hand side of eqn (9.7) is negligible in comparison to the dumping force, and the force term f_i is estimated using an underlying free-energy landscape.[80]

Classical MD simulations use force fields expressed in terms of energy functions $U(r)$ in order to reproduce molecular geometries and the time evolution of bond lengths, U_{bond}, and angles, U_{angle}, as well as non-bonding interactions, such as van der Waals, U_{vdW} and electrostatic U_{el}:[59,81]

$$U(r) = U_{\mathrm{bond}} + U_{\mathrm{angle}} + U_{\mathrm{vdW}} + U_{\mathrm{el}} \tag{9.8}$$

In the examples below both Langevin dynamics and force-field approaches were used. In contrast to the large number of studies reporting the experimental development of interpenetrating multi-network materials, or those using macroscopic models to characterize their response, there are very few reports investigating their synthesis and dynamics from a molecular coarse-grained perspective.

(i) Polymer–polymer hydrogels have been modeled at the MD level in small simulation volumes. Using a ''random walk reactive polymerization'' modeling method, the molecular structure of DN hydrogels made from a primary agar network and a secondary polyacrylamide (PAM) network was constructed *in silico*[82] (see Figure 9.5). The method consisted in simulating the formation of the physical primary network by self-assembling agar molecules into helical bundles, which were stabilized through hydrogen bonds. The secondary chemical

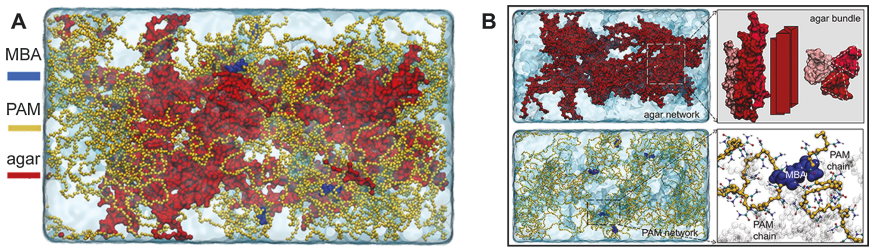

Figure 9.5 Simulations of the polymerization of an agar/polyacrylamide (PAM) double-network hydrogel. (A) Snapshot of the DN using a two-stage chain-growth polymerization. (B) Individual representations of the two networks (left) and details relevant to the two networks (right). Reproduced from ref. 82, https://doi.org/10.1038/s41524-021-00509-5, under the terms of the CC BY 4.0 license, https://creativecommons.org/licenses/by/4.0/.

network was later constructed in the presence of the primary agar network. Chain-growth polymerization of acrylamide was achieved using a random-walking reaction. *N*,*N*′-Methylenebisacrylamide (MBA) cross-linker molecules were added at random locations on the PAM network, followed by optimization for 100 ns at room temperature. This approach allowed for determination of the molecular structure of interpenetrating polymer–polymer DNs. These structures were also later used for structural analysis and to determine mechanical properties such as strain response, energy dissipation within the network and fracture.[82]

Another study used MD simulations to determine the mechanical and transport properties of poly(ethylene oxide)–poly(acrylic acid) (PEO–PAA) chemically cross-linked materials.[83] In this study, the authors used a force field that accounts for the effects of electrostatic, van der Waals, angle bending, bond-stretching, torsion and inversion components. The DN gels were built from PEO_{30} and PAA_{80} homopolymers. The 3-dimensional (3D) network structure was then produced by allowing the reactive ends of the two homopolymers to interact with each other (see Figure 9.6). Following cross-linking *in silico*, PEO–PAA hydrogels were exposed to uniaxial stress. Interestingly, the authors report that DN hydrogels have a sudden increase of stress above ~100% strain, which was higher than the summation of the stresses of the two respective single-networks (SN) at the same strain. This behavior resulted from the fact that PEO chains had to adopt more extended conformations in the DN compared to SN, as they must react with the PAA molecules during cross-linking. This expansion also led to a slightly higher water content in DN hydrogels, when compared to both SN PEO and PAA.

Other studies have also investigated *in silico* how individual components contribute to the overall properties of a multicomponent

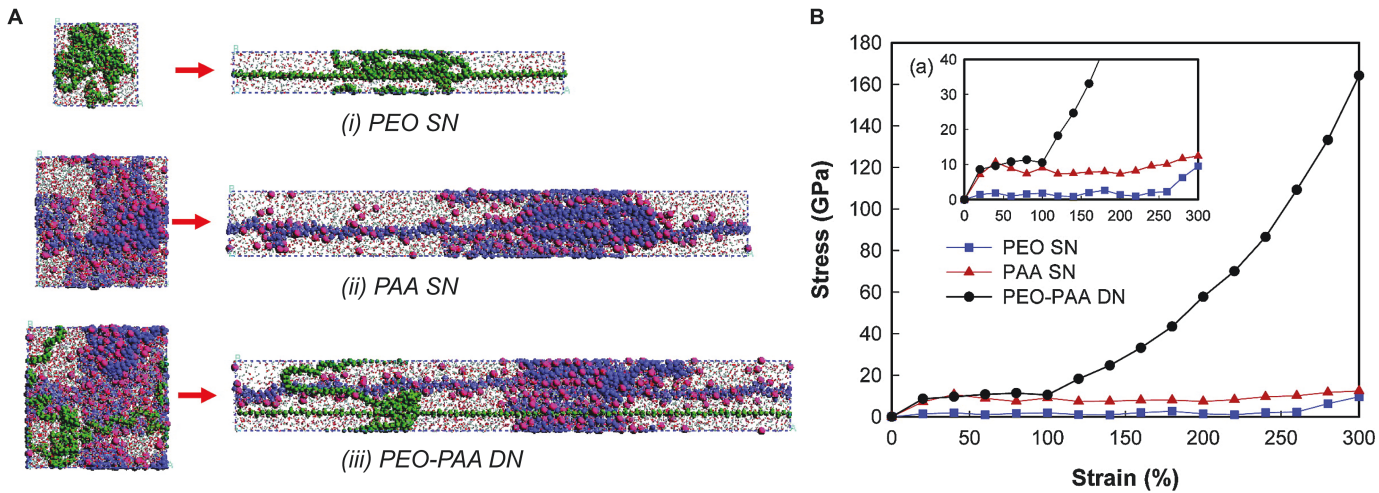

Figure 9.6 Molecular dynamics simulations of the mechanical properties of the PEO–PAA DN hydrogels and their individual components. (A) Equilibrated hydrogels (left) and their uniaxial extension to a strain of 300%. The PEO SN is shown in green, and the PAA SN in blue. The Na^+ ions are represented as pink spheres. (B) Calculated stress–strain curves of hydrogels. The stress in the DN increases rapidly above 100% strain, more than the sum of the individual components. Adapted from ref. 83 with permission from American Chemical Society, Copyright 2007.

polymeric hydrogel,[82] or how fracture propagates through a DN hydrogel,[84–86] or managed to predict elastic constants and material density from equilibrated structures.[87] For example, the effects of the composition and mechanical response of the individual networks on the overall fracture of a DN polymer–polymer material were investigated using coarse-grained molecular dynamics simulations[85] (see Figure 9.7). The authors determined the mechanical response of DN hydrogels made from a primary polymer network which is highly cross-linked and a secondary polymeric network which was cross-linked only slightly. By varying the ratio between these two networks, the authors determined that the primary network has a greater impact on Young's modulus, while the secondary network increased the peak stress and ductility. The simulations also revealed the sequence of events during network failure, with the highly cross-linked network extending and breaking first, followed by the disentanglement of the two networks and formation of void structures, connected together through the slightly connected secondary network.

(ii) Simulations of protein–polymer hydrogels have been used to rationally design synthetic materials with novel applications. These materials are important, as they can harvest from the broad spectrum of applications of proteins, and can also produce biocompatible materials. The most common approach for protein–polymer hydrogels uses polymer networks with proteins embedded inside.[88] Generally, proteins are either mixed with the monomers and cross-linker and fixated inside the network during polymerization, or adsorbed after the formation of the primary network. Polyacrylamide (PAM) gels imprinted with two model proteins, cytochrome complex and lysozyme, were studied using a coarse-grained approach.[89] The authors

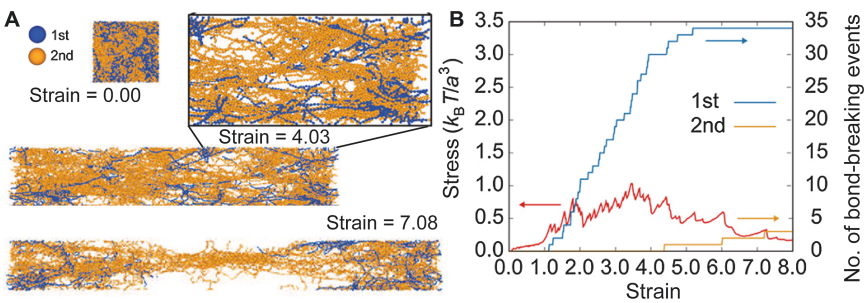

Figure 9.7 Fracture of the DN polymer–polymer gel made from interpenetrating networks. (A) Snapshots of the cross-sections of a DN gel made from a highly cross-linked primary network (blue) and a slightly cross-linked secondary network (orange) at various strains. (B) Stress and number of bond-breaking events as a function of strain determined from MD simulations. Adapted from ref. 85 with permission from American Chemical Society, Copyright 2018.

introduced a continuum simulation approach to describe molecular dynamics and the diffusion of proteins from the gel and to find how the diffusion mechanism of the two proteins differs with respect to their specific substrate-interactions.

A coarse-grained molecular dynamics modeling-based design was recently implemented to engineer self-assembled polymeric structures with active enzymes for hydrogel synthesis[90] (see Figure 9.8). The authors used PETase with styrene/2-vinylpyridine (2VP) random copolymers, which contain polar and charged groups, respectively. The challenge in this system is to limit the polymer–polymer aggregation, favoring polymer–protein non-bonded interactions. By controlling the copolymer fraction, simulations predicted the optimal ratio between charged and polar groups needed for the copolymer to encapsulate cytochrome redox-active protein. This study also showed that the assemblies between proteins and polymers are first promoted through hydrophobic interactions.

Multicomponent hydrogels in which the primary network is made out of proteins are less common. Such approaches were reported for proteins cross-linked chemically at specific exposed amino acids and reacting with other proteins, polyelectrolytes, small ions or peptides

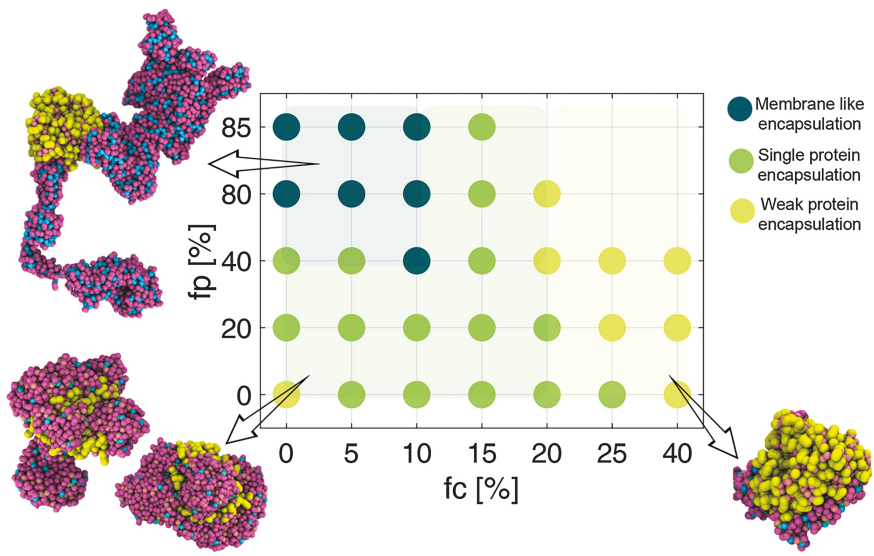

Figure 9.8 Phase diagram of polymer–P450 enzyme complexes obtained with MD simulations. Adjustment in the polar (fp) and charged (fc) fractions of the copolymer structure results in three co-assembly modes: a membrane-like co-assembly (dark green dots and top-left structure), a single-protein encapsulation (light green dots and bottom-left structure) and a weak protein encapsulation (yellow dots and right structure). Reproduced from ref. 90 with permission from American Chemical Society, Copyright 2021.

of opposite charge.[20,22,91,92] Due to the large number of different atoms forming the structure of a protein domain, the models developed thus far use a coarse-grained approach, with each protein domain represented as an individual entity.[17,39,93,94] Proteins can be formed by single or multiple domains, which are typically globular and produce well-defined maximum connections-per-domain. For example, gelation of protein hydrogels made from octameric repeats was studied using a coarse-grained approach[17] (see Figure 9.9). In this case, protein molecules, represented as beads-on-a-string, were placed in a unit volume and left to diffuse and cross-link. An interesting aspect of hydrogels with globular proteins as their primary network comes from their response to force. The tertiary structure of proteins is formed by alpha-helices and beta-strands, which can break under force. When the hydrogen bonds holding the tertiary folded structure of a domain break, the protein transitions from a globular structure into an extended polypeptide chain, in a process

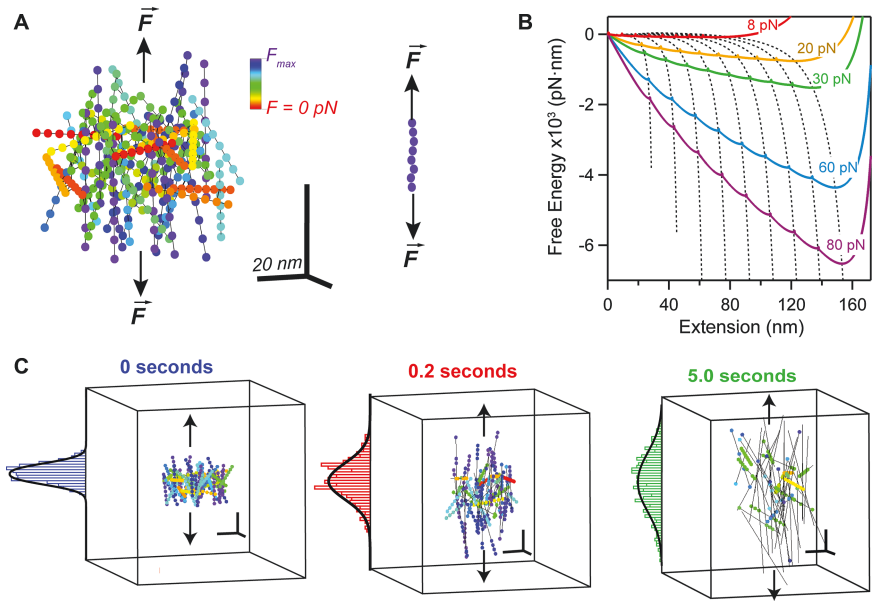

Figure 9.9 Model of the response of polyprotein hydrogels, as they unfold under a force vector. (A) Representation of a protein hydrogel before application of force (left) and of a single polyprotein (right). The color code represents the experienced force for each molecule, which depends on their orientation. (B) Projection of the free energy landscape on the pulling coordinate for a polyprotein with eight repeats at various forces along the N-to-C coordinate, showing an accordionlike shape. Dotted lines follow local energy minima. (C) Snapshots of the same gel at three different time points, showing the orientation of molecules and unfolding of protein domains along an axial coordinate. Adapted from ref. 17 with permission from APS, Copyright 2018.

known as unfolding. Hence under force, the molecules first align to the pulling direction and then domains inside the molecule can unfold and release ''hidden'' lengths. This process happens faster as force is increased, while the extension of the unfolded polypeptide chain follows polymer elasticity principles, as shown in Figure 9.4A. The unfolding and refolding processes under a force vector may play an important role *in vivo*[95] and can be efficiently modeled using energy landscapes[17,80,96] (Figure 9.9B). As proteins typically require higher forces to unfold than to refold, and the unfolding extension is larger than the refolding contraction, a hysteresis is measured both experimentally and from simulations in stress–strain curves.[23] Interestingly for protein-based hydrogels, the hysteresis can be removed when the material is immersed in a solution that can chemically denature the folded domains, making the material response purely elastic.[23] Using this simple modeling approach, the single molecule unfolding and alignment of proteins to a force vector was scaled to the macroscopic response of the protein-based biomaterial (Figure 9.9C).

(iii) Polymer–inclusion hydrogels are typically easier to model, as the inclusions have a well-defined structure, such as a crystalline arrangement or a small inelastic sphere/cylinder. These components are usually static during the simulation. For example, MD simulations were used to describe graphene-based composites.[97] Graphene makes ordered crystalline sheets that are functionalized by macromolecules, which simplifies the simulation environment. The glass transition temperature[98] and molecular mobility of the components[99] were estimated from coarse-grained simulations of polyethylene (PE)/graphene composites. Similarly, the structural and dynamical properties of polymethyl methacrylate (PMMA)/graphene composites were described using coarse-grained approaches.[100]

Other nanoscale approaches involve polymer nanocomposites, such as epoxy/alumina nanoparticles (see Figure 9.10A).[101] In this study, the authors used MD simulations to investigate the effect of the size of alumina nanoparticles on the overall mechanical properties of an epoxy-based composite. A spherical alumina bead of desired size was placed in the center of the simulation volume, and then cross-linking was done by independently modeling the epoxy resin and curing agents. The mechanical properties were then calculated using the Parrinello–Rahman fluctuation method[102] and showed a strong dependency of Young's and shear moduli on the particle radius and degree of cross-linking (see Figure 9.10B).

Polymer–nanoclay composites have also been simulated at various scales.[103–105] Instead of particles imbedded in polymeric matrices, clays have nanometer-scaled sheets. These sheets give rigidity to the multicomponent material, while the sandwiched polymer gives flexibility.[106] One study used a multi-scale approach to describe the

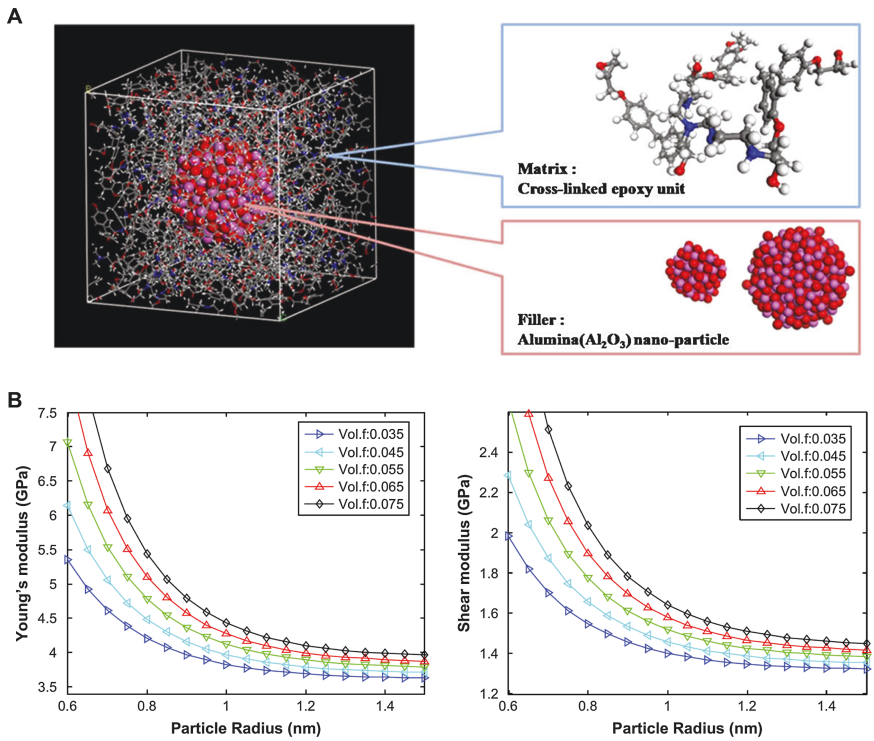

Figure 9.10 Modeling of cross-linked epoxy nanocomposites. (A) Snapshot of the nanocomposite's unit cell consisting of alumina particles and a cross-linked epoxy matrix. (B) Estimated Young's modulus and shear modulus as a function of particle radius for composites with varying volume fractions of particles. Adapted from ref. 101 with permission from Elsevier, Copyright 2009.

dynamics of intercalation between poly(ethylene glycol) (PEG) and poly(vinyl alcohol) (PVA) and clay nanoparticles arranged in sheets[104] (see Figure 9.11). The authors produced coarse-grained representations that maintained specific chemical interactions. These chemical interactions were determined using quantum and atomistic approaches. Interestingly, the authors found that while the polymer molecules intercalate with the clay sheet, they are forced from their naturally collapsed conformation into an extended state, and sometimes bridge between non-consecutive clay layers (see Figure 9.11).

(iv) Void-double network hydrogels deserve consideration due to their capacity to generate porous homogeneous materials, with applications in cell growth and separation of larger molecules. A recent study investigated the formation of aggregation centers for the secondary network, which compete with the cross-linking of a protein-based primary network (see Figure 9.12).[39] Such a system was

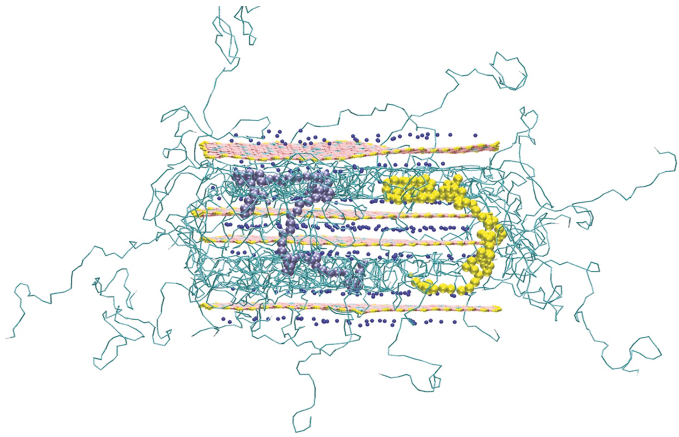

Figure 9.11 Clay–PVA polymer composites. Side view from simulation of a tactoid showing some bending of clay sheet and extension of PVA polymer molecules while the system has been equilibrated. Two PVA molecules that connect non-adjacent clay layers, preventing intercalation in the middle layer, are shown in yellow and purple. Reproduced from ref. 104, https://doi.org/10.1002/adma.201403361, under the terms of the CC BY 4.0 license, https://creativecommons.org/licenses/by/4.0/.

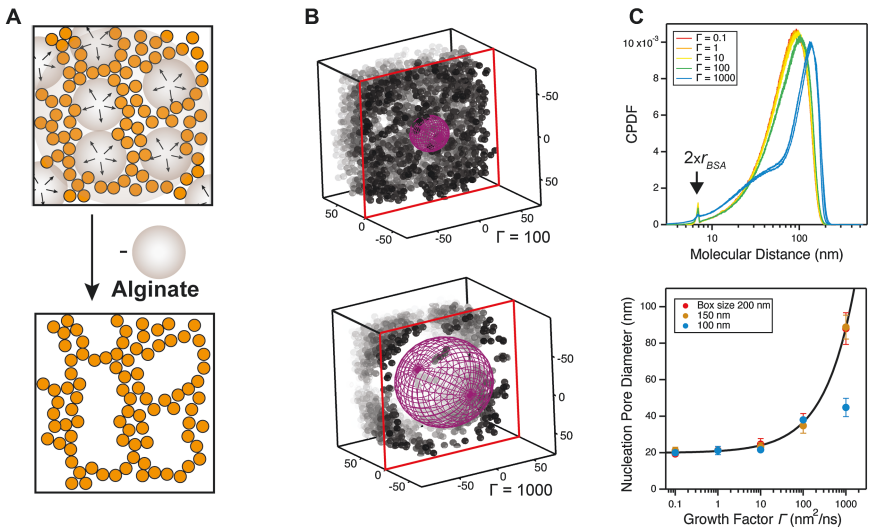

Figure 9.12 Simulations of the formation of BSA void-DN hydrogels. (A) Schematics of the approach, where Ca^{2+}-induced alginate aggregation centers compete with the formation of the primary BSA protein network (top) and resulting pores after alginate clusters are dissolved (bottom). (B) Sliced of snapshots of two hydrogels with the same concentration of BSA but different aggregation rates for a central alginate aggregate. (C) Quantification of the pore size as a function of the alginate aggregation rate for various simulation box sizes using (top): the cumulative probability distribution function (CPDF) and (bottom): largest inoculated sphere methods. Adapted from ref. 39 with permission from American Chemical Society, Copyright 2022.

developed experimentally using the aggregation of alginate in the presence of Ca^{2+} ions in parallel with the cross-linking of BSA, a globular monomeric protein.[39] The formation of the primary protein network was simulated using a coarse-grained approach, where spheres with radii equal to that of BSA protein were placed in a simulation volume at concentrations similar to those used experimentally. While the spheres were left to diffuse and connect to form the primary hydrogel network, a repulsive force field was activated in the center of the simulation volume. The intensity of this repulsive field was varied and represented the aggregation rate of the secondary alginate network. The formed pore was then estimated from the largest sphere that could be inoculated inside the gel structure. The porosity was then estimated from both the cumulative probability distribution function (CPDF) of protein molecules and the largest inoculated sphere. These simulations demonstrate that the nucleation growth rate of alginate drives the pore-formation process and a fast aggregation rate is required to generate pores throughout the material using this competitive crosslinking approach.

9.5 Conclusions and Outlook

In this chapter, we reviewed the main classes of multicomponent hydrogels from the perspective of macroscopic and nanoscopic modeling approaches. Among these classes, polymer–polymer hydrogels are the most experimentally and theoretically developed. Modeling of protein–polymer materials requires the use of knowledge related to the folded tertiary structure of proteins, as well as implementation of their unfolding response. Polymer–inclusion multi-materials have also been extensively modeled with MD simulations. Inclusions typically have crystalline structures, which makes it easier to model them. Finally, the synthesis and viscoelastic response of void–polymer hydrogels were discussed.

Modeling and simulations of multicomponent hydrogels require a multiscale approach and improvements in resolution and accuracy come at the expense of computational time. One of the most challenging aspects of modeling multicomponent materials is transitioning between different scales.[107] This transitioning needs to take into account phenomena that are specific for a given scale and to balance accuracy with efficiency. One typical approach is to sequentially transition from a small to a large scale.[104,108] Concurrent scaling approaches have also been developed, mainly when studying crack propagation in materials. In these methods, the interface of the crack was analyzed at finer resolution than the rest of the material.[109,110] Adaptive resolution approaches combine all-atomistic and coarse-grained descriptions of subregions, separated by smooth transition boundaries.[111,112] More recently, with the advent of artificial intelligence and big data science, machine learning is becoming an increasingly important tool to integrate data over several scales.[113] Machine learning can reveal

correlations identified by multiscale modeling and assign uncertainty to mechanisms identified through simulations.

With the continuous improvements in computational technology and the growing database of multicomponent hydrogels, modeling approaches are becoming increasingly more accurate and reliable. They are an invaluable tool for designing novel materials with unique properties and to investigate scaling in networks and biological tissues.

Acknowledgements

The author acknowledges funding support from the NSF (grant no. MCB-1846143 and DBI-1919670) and Greater Milwaukee Foundation (Shaw award).

References

1. M. A. Haque, T. Kurokawa and J. P. Gong, *Polymer*, 2012, **53**, 1805–1822.
2. X. Liu, Z. Ren, F. Liu, L. Zhao, Q. Ling and H. Gu, *ACS Appl. Mater. Interfaces*, 2021, **13**, 14612–14622.
3. X. G. Wang, F. Zhao, B. Pang, X. P. Qin and S. Y. Feng, *RSC Adv.*, 2018, **8**, 6789–6797.
4. H. K. Lau and K. L. Kiick, *Biomacromolecules*, 2015, **16**(1), 28–42.
5. Y. Huang, M. Zhong, Y. Huang, M. Zhu, Z. Pei, Z. Wang, Q. Xue, X. Xie and C. Zhi, *Nat. Commun.*, 2015, **6**, 10310.
6. M. J. Buehler, S. Keten and T. Ackbarow, *Prog. Mater. Sci.*, 2008, **53**, 1101–1241.
7. Y. Kawauchi, Y. Tanaka, H. Furukawa, T. Kurokawa, T. Nakajima, Y. Osada and J. P. Gong, *J. Phys.: Conf. Ser.*, 2009, **184**, 012016.
8. J. P. Gong, *Soft Matter*, 2010, **6**, 2583–2590.
9. Y. Tang, X. Zhang, X. Li, C. Ma, X. Chu, L. Wang and W. Xu, *Eur. Polym. J.*, 2022, **162**, 110881.
10. A. K. Patterson and D. K. Smith, *Chem. Commun.*, 2020, **56**, 11046–11049.
11. X. Jia and K. L. Kiick, *Macromol. Biosci.*, 2009, **9**, 140–156.
12. O. Chaudhuri, L. Gu, D. Klumpers, M. Darnell, S. A. Bencherif, J. C. Weaver, N. Huebsch, H. P. Lee, E. Lippens, G. N. Duda and D. J. Mooney, *Nat. Mater.*, 2016, **15**, 326–334.
13. B. O. Okesola, Y. Wu, B. Derkus, S. Gani, D. Wu, D. Knani, D. K. Smith, D. J. Adams and A. Mata, *Chem. Mater.*, 2019, **31**, 7883–7897.
14. D. A. Murguía-Flores, J. Bonilla-Ríos, M. R. Canales-Fiscal and A. Sánchez-Fernández, *Chem. Cent. J.*, 2016, **10**, 26.
15. S. Tizchang, M. S. Khiabani, R. R. Mokarram, H. Hamishehkar, N. S. Mohammadi and Y. Chisti, *Biochim. Biophys. Acta, Gen. Subj.*, 2021, **1865**, 129896.
16. S. Lv, D. M. Dudek, Y. Cao, M. M. Balamurali, J. Gosline and H. Li, *Nature*, 2010, **465**, 69–73.

17. K. Shmilovich and I. Popa, *Phys. Rev. Lett.*, 2018, **121**, 168101.
18. J. Wu, P. Li, C. Dong, H. Jiang, X. Bin, X. Gao, M. Qin, W. Wang, C. Bin and Y. Cao, *Nat. Commun.*, 2018, **9**, 620.
19. Q. Bian, L. Fu and H. Li, *Nat. Commun.*, 2022, **13**, 137.
20. L. R. Khoury and I. Popa, *Nat. Commun.*, 2019, **10**, 5439.
21. M. A. Gonzalez, J. R. Simon, A. Ghoorchian, Z. Scholl, S. Lin, M. Rubinstein, P. Marszalek, A. Chilkoti, G. P. López and X. Zhao, *Adv. Mater.*, 2017, **29**, 1604743.
22. L. R. Khoury, M. Slawinski, D. R. Collison and I. Popa, *Sci. Adv.*, 2020, **6**, eaba6112.
23. L. R. Khoury, J. Nowitzke, K. Shmilovich and I. Popa, *Macromolecules*, 2018, **51**, 1441–1452.
24. N. Lin, J. Huang and A. Dufresne, *Nanoscale*, 2012, **4**, 3274–3294.
25. K. J. De France, T. Hoare and E. D. Cranston, *Chem. Mater.*, 2017, **29**, 4609–4631.
26. S. Bhattacharya and S. K. Samanta, *Chem. Rev.*, 2016, **116**, 11967–12028.
27. H. Wang, Q. Chen and S. Zhou, *Chem. Soc. Rev.*, 2018, **47**, 4198–4232.
28. A. J. Clasky, J. D. Watchorn, P. Z. Chen and F. X. Gu, *Acta Biomater.*, 2021, **122**, 1–25.
29. P. Makvandi, A. Zarepour, X. Zheng, T. Agarwal, M. Ghomi, R. Sartorius, E. N. Zare, A. Zarrabi, A. Wu, T. K. Maiti, B. R. Smith, R. S. Varma, F. R. Tay and V. Mattoli, *Appl. Mater. Today*, 2021, **24**, 101107.
30. Y. Li, G. Huang, X. Zhang, B. Li, Y. Chen, T. Lu, T. J. Lu and F. Xu, *Adv. Funct. Mater.*, 2013, **23**, 660–672.
31. V. F. Cardoso, A. Francesko, C. Ribeiro, M. Bañobre-López, P. Martins and S. Lanceros-Mendez, *Adv. Healthcare Mater.*, 2018, **7**, 1700845.
32. W.-C. Lin, W. Fan, A. Marcellan, D. Hourdet and C. Creton, *Macromolecules*, 2010, **43**, 2554–2563.
33. M. Takafuji, S.-Y. Yamada and H. Ihara, *Chem. Commun.*, 2011, **47**, 1024–1026.
34. K. Haraguchi, T. Takehisa and S. Fan, *Macromolecules*, 2002, **35**, 10162–10171.
35. K. Haraguchi, *Curr. Opin. Solid State Mater. Sci.*, 2007, **11**, 47–54.
36. T. Nakajima, H. Furukawa, Y. Tanaka, T. Kurokawa and J. P. Gong, *J. Polym. Sci., Part B: Polym. Phys.*, 2011, **49**, 1246–1254.
37. N. Huebsch, E. Lippens, K. Lee, M. Mehta, S. T. Koshy, M. C. Darnell, R. M. Desai, C. M. Madl, M. Xu, X. Zhao, O. Chaudhuri, C. Verbeke, W. S. Kim, K. Alim, A. Mammoto, D. E. Ingber, G. N. Duda and D. J. Mooney, *Nat. Mater.*, 2015, **14**, 1269–1277.
38. Q. Q. Dou, Z. W. K. Low, K. Y. Zhang and X. J. Loh, *RSC Adv.*, 2017, **7**, 27449–27453.
39. M. Slawinski, L. R. Khoury, S. Sharma, J. Nowitzke, J. H. Gutzman and I. Popa, *ACS Biomater. Sci. Eng.*, 2022, **8**, 1132–1142.
40. J. Yang, K. Li, C. Tang, Z. Liu, J. Fan, G. Qin, W. Cui, L. Zhu and Q. Chen, *Adv. Funct. Mater.*, 2022, **32**, 2110244.

41. L. R. Khoury, J. Nowitzke, N. Dahal, K. Shmilovich, A. Eis and I. Popa, *J. Vis. Exp.*, 2018, **138**, 58280.
42. A. Gooneie, S. Schuschnigg and C. Holzer, *Polymers*, 2017, **9**, 16.
43. F. Zhonggang, K. Tadashi, N. Takao, S. Daisuke, K. Tatsuo and U. Mitsuo, *AIMS Mater. Sci.*, 2017, **4**, 680–705.
44. V. Annarasa, A. A. Popov and D. S. A. De Focatiis, *Mech. Time-Depend. Mater.*, 2020, **24**, 463–479.
45. A. R. Cioroianu, E. M. Spiesz and C. Storm, *J. Mech. Phys. Solids*, 2016, **89**, 110–125.
46. E. M. Arruda and M. C. Boyce, *J. Mech. Phys. Solids*, 1993, **41**, 389–412.
47. F. Meng, R. H. Pritchard and E. M. Terentjev, *Macromolecules*, 2016, **49**, 2843–2852.
48. S. Nam, K. H. Hu, M. J. Butte and O. Chaudhuri, *Proc. Natl. Acad. Sci.*, 2016, **113**, 5492–5497.
49. Y. Li, Z. Liu, Z. Jia, W. K. Liu, S. M. Aldousari, H. S. Hedia and S. A. Asiri, *Comput. Mech.*, 2017, **59**, 187–201.
50. Y. Togashi and H. Flechsig, *Int. J. Mol. Sci.*, 2018, **19**, 3899.
51. S. Kmiecik, D. Gront, M. Kolinski, L. Wieteska, A. E. Dawid and A. Kolinski, *Chem. Rev.*, 2016, **116**, 7898–7936.
52. H. I. Ingolfsson, C. A. Lopez, J. J. Uusitalo, D. H. de Jong, S. M. Gopal, X. Periole and S. J. Marrink, *Wiley Interdiscip. Rev.: Comput. Mol. Sci.*, 2014, **4**, 225–248.
53. S. J. Marrink, H. J. Risselada, S. Yefimov, D. P. Tieleman and A. H. de Vries, *J. Phys. Chem. B*, 2007, **111**, 7812–7824.
54. X. Periole and S. J. Marrink, *Methods Mol. Biol.*, 2013, **924**, 533–565.
55. W. Shinoda, R. Devane and M. L. Klein, *Mol. Simul.*, 2007, **33**, 27–36.
56. A. R. Leach, *Molecular modelling: principles and applications*, Prentice Hall, Harlow, England, New York, 2001.
57. R. Alessandri, F. Grünewald and S. J. Marrink, *Adv. Mater.*, 2021, **33**, 2008635.
58. T. Casalini, V. Limongelli, M. Schmutz, C. Som, O. Jordan, P. Wick, G. Borchard and G. Perale, *Front. Bioeng. Biotechnol.*, 2019, **7**, DOI: 10.3389/fbioe.2019.00268.
59. G. Fitzgerald, J. DeJoannis and M. Meunier, in *Modeling, Characterization, and Production of Nanomaterials*, ed. V. K. Tewary and Y. Zhang, Woodhead Publishing, 2015, pp. 3–53.
60. S. Park and Y. Chen, Mechanics of biological systems, *Introduction to mechanobiology and experimental techniques*, Morgan & Claypool Publishers, 2019.
61. W. Kuhn, *Kolloid-Z.*, 1934, **68**, 2–15.
62. A. Nakayama, A. Kakugo, J. P. Gong, Y. Osada, M. Takai, T. Erata and S. Kawano, *Adv. Funct. Mater.*, 2004, **14**, 1124–1128.
63. J. P. Gong, Y. Katsuyama, T. Kurokawa and Y. Osada, *Adv. Mater.*, 2003, **15**, 1155–1158.
64. D. Myung, W. Koh, J. Ko, Y. Hu, M. Carrasco, J. Noolandi, C. N. Ta and C. W. Frank, *Polymer*, 2007, **48**, 5376–5387.

65. V. Vogel and M. Sheetz, *Nat. Rev. Mol. Cell Biol.*, 2006, **7**, 265–275.
66. A. R. Bausch, F. Ziemann, A. A. Boulbitch, K. Jacobson and E. Sackmann, *Biophys. J.*, 1998, **75**, 2038–2049.
67. D. Klatt, U. Hamhaber, P. Asbach, J. Braun and I. Sack, *Phys. Med. Biol.*, 2007, **52**, 7281–7294.
68. G. Mattei and A. Ahluwalia, *Acta Biomater.*, 2016, **45**, 60–71.
69. S. Park, Y. K. Joo and Y. Chen, *Sci. Rep.*, 2019, **9**, 13286.
70. M. Aghvami, K. L. Billiar and E. A. Sander, *J. Biomech. Eng.*, 2016, **138**, 1010061–10100611.
71. A. E. Brown, R. I. Litvinov, D. E. Discher, P. K. Purohit and J. W. Weisel, *Science*, 2009, **325**, 741–744.
72. A. Sharma, A. J. Licup, K. A. Jansen, R. Rens, M. Sheinman, G. H. Koenderink and F. C. MacKintosh, *Nat. Phys.*, 2016, **12**, 584–587.
73. Q. Wang and Z. Gao, *J. Mech. Phys. Solids*, 2016, **94**, 127–147.
74. V. Ganesan and A. Jayaraman, *Soft Matter*, 2014, **10**, 13–38.
75. D. Caccavo, G. Lamberti and A. A. Barba, *Eur. J. Pharm. Biopharm.*, 2020, **152**, 299–306.
76. J. Narayanan, J.-Y. Xiong and X.-Y. Liu, *J. Phys.: Conf. Ser.*, 2006, **28**, 83–86.
77. A. P. Balgude, X. Yu, A. Szymanski and R. V. Bellamkonda, *Biomaterials*, 2001, **22**, 1077–1084.
78. B. Xue, D. Tang, X. Wu, Z. Xu, J. Gu, Y. Han, Z. Zhu, M. Qin, X. Zou, W. Wang and Y. Cao, *Proc. Natl. Acad. Sci. U. S. A.*, 2021, **118**, e2110961118.
79. M. Sauerwein and H. Steeb, *Int. J. Eng. Sci.*, 2020, **155**, 103353.
80. R. Berkovich, S. Garcia-Manyes, M. Urbakh, J. Klafter and J. M. Fernandez, *Biophys. J.*, 2010, **98**, 2692–2701.
81. W. D. Cornell, P. Cieplak, C. I. Bayly, I. R. Gould, K. M. Merz, D. M. Ferguson, D. C. Spellmeyer, T. Fox, J. W. Caldwell and P. A. Kollman, *J. Am. Chem. Soc.*, 1995, **117**, 5179–5197.
82. M. Z. Zhang, D. Zhang, H. Chen, Y. X. Zhang, Y. L. Liu, B. P. Ren and J. Zheng, *npj Comput. Mater.*, 2021, **7**, DOI: 10.1038/s41524-021-00509-5.
83. S. S. Jang, W. A. Goddard and M. Y. S. Kalani, *J. Phys. Chem. B*, 2007, **111**, 1729–1737.
84. J. Tauber, L. Rovigatti, S. Dussi and J. van der Gucht, *Macromolecules*, 2021, **54**, 8563–8574.
85. Y. Higuchi, K. Saito, T. Sakai, J. P. Gong and M. Kubo, *Macromolecules*, 2018, **51**, 3075–3087.
86. R. Zhao, Y. Wang and X. Gong, *Polymer*, 2022, **244**, 124670.
87. C. Wu and W. Xu, *Polymer*, 2007, **48**, 5802–5812.
88. M. E. Byrne, K. Park and N. A. Peppas, *Adv. Drug Delivery Rev.*, 2002, **54**, 149–161.
89. I. Zadok and S. Srebnik, *J. Phys. Chem. B*, 2018, **122**, 7091–7101.
90. A. Cardellini, F. Jiménez-Ángeles, P. Asinari and M. Olvera de la Cruz, *ACS Nano*, 2021, **15**, 16139–16148.
91. M. A. Gonzalez, J. R. Simon, A. Ghoorchian, Z. Scholl, S. Lin, M. Rubinstein, P. Marszalek, A. Chilkoti, G. P. Lopez and X. Zhao, *Adv. Mater.*, 2017, **29**, 1604743.

92. Q. Bian, L. Fu and H. Li, *Nat. Commun.*, 2022, **13**, 137.
93. A. Aufderhorst-Roberts, M. D. G. Hughes, A. Hare, D. A. Head, N. Kapur, D. J. Brockwell and L. Dougan, *Biomacromolecules*, 2020, **21**, 4253–4260.
94. B. S. Hanson and L. Dougan, *Macromolecules*, 2020, **53**, 7335–7345.
95. S. Sharma, S. Subramani and I. Popa, *FEBS J.*, 2021, **288**, 1742–1758.
96. R. Berkovich, R. I. Hermans, I. Popa, G. Stirnemann, S. Garcia-Manyes, B. J. Berne and J. M. Fernandez, *Proc. Natl. Acad. Sci. U. S. A.*, 2012, **109**, 14416–14421.
97. D. G. Papageorgiou, I. A. Kinloch and R. J. Young, *Prog. Mater. Sci.*, 2017, **90**, 75–127.
98. Y.-Z. Sheng, H. Yang, J.-Y. Li and M. Sun, *Chem. Res. Chin. Univ.*, 2013, **29**, 788–792.
99. T. Zheng, S. Wang, L. Zhou, X. Li and H. Zhang, *Appl. Surf. Sci.*, 2022, **580**, 152301.
100. A. N. Rissanou and V. Harmandaris, *J. Nanopart. Res.*, 2013, **15**, 1589.
101. S. Yu, S. Yang and M. Cho, *Polymer*, 2009, **50**, 945–952.
102. M. Parrinello and A. Rahman, *J. Chem. Phys.*, 1982, **76**, 2662–2666.
103. J. L. Suter, R. L. Anderson, H. Christopher Greenwell and P. V. Coveney, *J. Mater. Chem.*, 2009, **19**, 2482–2493.
104. J. L. Suter, D. Groen and P. V. Coveney, *Adv. Mater.*, 2015, **27**, 966–984.
105. G. Scocchi, P. Posocco, M. Fermeglia and S. Pricl, *J. Phys. Chem. B*, 2007, **111**, 2143–2151.
106. O. L. Manevitch and G. C. Rutledge, *J. Phys. Chem. B*, 2004, **108**, 1428–1435.
107. Y. Li, B. C. Abberton, M. Kröger and W. K. Liu, *Polymers*, 2013, **5**, 751–832.
108. J. R. Brown, Y. Seo, T. A. D. Maula and L. M. Hall, *J. Chem. Phys.*, 2016, **144**, 124904.
109. J. Q. Broughton, F. F. Abraham, N. Bernstein and E. Kaxiras, *Phys. Rev. B: Condens. Matter Mater. Phys.*, 1999, **60**, 2391–2403.
110. R. E. Miller and E. B. Tadmor, *Modell. Simul. Mater. Sci. Eng.*, 2009, **17**, 053001.
111. W. A. Curtin and R. E. Miller, *Modell. Simul. Mater. Sci. Eng.*, 2003, **11**, R33–R68.
112. M. Praprotnik, L. D. Site and K. Kremer, *J. Chem. Phys.*, 2005, **123**, 224106.
113. M. Alber, A. Buganza Tepole, W. R. Cannon, S. De, S. Dura-Bernal, K. Garikipati, G. Karniadakis, W. W. Lytton, P. Perdikaris, L. Petzold and E. Kuhl, *npj Digital Med.*, 2019, **2**, 115.